Unfolding the hippocampus: an intrinsic coordinate system for subfield segmentations and quantitative mapping

Jordan DeKraker[1,2,3], Kayla M. Ferko[1,2,3], Jonathan C. Lau[2,4,5], Stefan Köhler[1,6]*, Ali R. Khan[2,7,8]*

[1] Brain and Mind Institute, University of Western Ontario, London, Ontario, Canada

[2] Imaging Research Laboratories, Robarts Research Institute, University of Western Ontario, London, Ontario, Canada

[3] Graduate Program in Neuroscience, University of Western Ontario, London, Ontario, Canada

[4] Graduate Program in Biomedical Engineering, University of Western Ontario, London, Ontario, Canada

[5] Division of Neurosurgery, Department of Clinical Neurological Sciences, London Health Sciences Centre, University Hospital, University of Western Ontario, London, Ontario, Canada

[6] Department of Psychology, University of Western Ontario, London, Ontario, Canada

[7] Department of Medical Biophysics, Schulich School of Medicine and Dentistry, University of Western Ontario, London, Ontario, Canada

[8] Department of Medical Imaging, Schulich School of Medicine and Dentistry, University of Western Ontario, London, Ontario, Canada

* Co-senior authors: contributed equally to the supervision of this study

Abstract

The hippocampus, like the neocortex, has a morphological structure that is complex and variable in its folding pattern, especially in the hippocampal head. The current study presents a computational method to unfold hippocampal grey matter, with a particular focus on the hippocampal head where complexity is highest due to medial curving of the structure and the variable presence of digitations. This unfolding was performed on segmentations from high-resolution, T2-weighted 7T MRI data from 12 healthy participants and one surgical patient whose resected hippocampal tissue was used for histological validation. We traced a critical image feature known as the hippocampal 'dark band' in these images, then employed user-guided semi-automated techniques to detect and subsequently unfold the surrounding hippocampal grey matter. This unfolding was done by solving Laplace's equation in three dimensions of interest: longitudinal, proximal-distal, and laminar. The resulting 'unfolded coordinate space' provides an intuitive way of mapping the hippocampal subfields in 2D space (longitudinal and proximal-distal), such that similar borders can be applied in the head, body, and tail of the hippocampus independently of cross-participant variability in folding. Examination of a histological sample reveals that our unfolded coordinate system shows biological validity, and that subfield segmentations applied in this space are able to capture features not seen in manual tracing protocols. This unfolding method can also provide a standardized space for mapping tissue properties; for illustration we map hippocampal intra-cortical myelin and thickness in relation to subfield borders.

Research highlights

- Dark band in hippocampal head consistently detected with 7T, T2 isotropic MRI
- Hippocampal grey matter unfolded using Laplace's equation in 3D
- Unfolded subfields capture critical structural elements and agree with histology
- Intracortical myelin and thickness mapped in unfolded coordinate space

Keywords

Hippocampus, Hippocampal subfields, Uncus, Magnetic Resonance Imaging, 7 Tesla, Ultra-high field MRI, Morphometry, Segmentation, Computational Anatomy

1. Introduction

Researchers often distinguish the hippocampus from neocortex but the hippocampus, in fact, also has a cortical composition sometimes referred to as archicortex due to its wide evolutionary preservation (e.g. Duvernoy *et al.*, 2013). Like the neocortex, the hippocampus shows variable gyrification, often referred to as digitations or pseudo-digitations in the anterior hippocampal head and more posterior body/tail, respectively. This creates major challenges for cross-participant alignment and parcellation. This is particularly of interest given the recent controversy over parcellation of the hippocampus into subfields in MR data, which are not sensitive to cytoarchitectonic features that define the subfields (for an overview of this controversy see Yushkevich *et al.*, 2015a and harmonization efforts by Wisse *et al.*, 2017).

Though present in the rest of the hippocampus, digitations are most prominent in the hippocampal head. This has created a major challenge for subfield segmentation protocols and as such most protocols do not segment this region, or do not honour its complex and variable structure (see Yushkevich *et al.*, 2015a). Recently, following a detailed histological characterization of the human hippocampal head by Ding & Van Hoesen (2015), Dalton *et al.* (2017) and also Berron *et al*. (2017) presented a protocol for manually segmenting the subfields of the hippocampal head using geometric rules and descriptions in 2D coronal slices, which captures many key structural features. However, like other protocols limited to 2D slice viewing and geometric rules, these protocols simplify subfield structure in the uncus and cannot easily account for inter-individual variability in folding (i.e. digitations) or other differences in morphology (e.g. dysplasias or more subtle differences in orientation or position within the medial-temporal lobe), which are issues in inter-subject alignment rather than in defining subfield borders *per se*.

1.1 Structural features of the hippocampal head

Subfield borders show greatest disagreement across tracing protocols in the hippocampal head, which is a major concern given that the hippocampal head represents nearly half of the geodesic length of the hippocampus (Duvernoy *et al.*, 2013), and has been suggested to exhibit shared as well as unique functional features with the rest of the hippocampus (Poppenk *et al.*, 2013; Zeidman and Maguire, 2016). Recent evidence from Ding & Van Hoesen (2015) offers a new morphological characterization of this structure. Their study examined densely sampled coronal slices along the length of the hippocampal head in several different *ex-vivo* specimens. A main finding in this characterization was the documentation of considerable

interindividual differences in digitations (i.e. folding, similar to the gyrification of neocortex) in the hippocampal head, varying from 2 to 4 digitations, with additional pseudo-digitations sometimes found along the lateral and inferior sides of the hippocampal body and tail. Ding & Van Hoesen also delineated the subfields in detail in the uncus- a part of the hippocampal head that curves medially, posteriorly, and superiorly (see Figure 1B). In line with Duvernoy *et al.*'s (2013) characterization, Ding & Van Hoesen showed that all subfields of the hippocampus, including the subiculum, contiguously follow this curvature through the hippocampal head and have their natural anterior termination not in the absolute anterior tip of the hippocampus, but rather in the more medial and posterior vertical (i.e. upward curving) component of the uncus (Figure 1B). As the subfields curve into the uncus, their borders also shift such that in the most anterior portions, the subiculum moves from a position on the inferior side, as in the body of the hippocampus, to a position that wraps around the anterior and superior sides. In other words, the archicortical 'roll' or folding in the proximal-distal dimension appears to be higher here. Finally, in the more medial vertical component of the uncus, the subfields appear to flatten out along the proximal-distal dimension before contacting neighbouring hippocampal-amygdala transition area (HATA) and entorhinal cortex. A detailed segmentation of this region should capture each of these features, and here we aim to provide a tool with sufficient validity and precision to index these structural complexities.

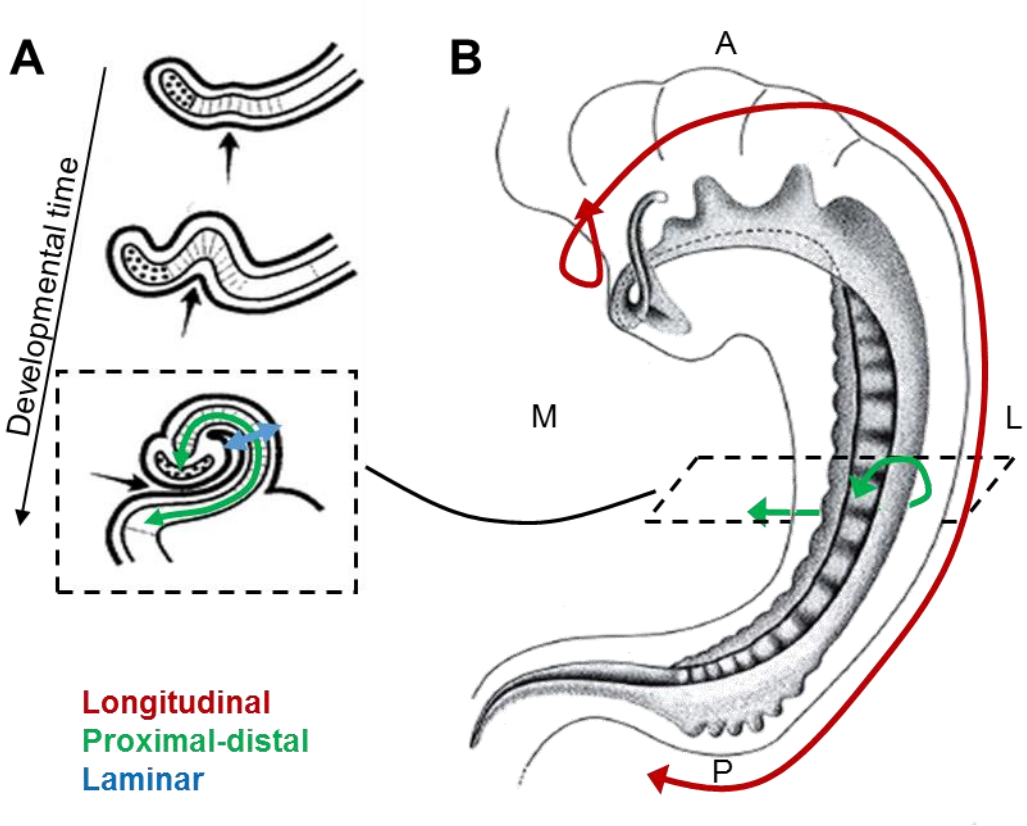

Figure 1 <1.5 column width, coloured>. Ontogeny and anatomy of the hippocampus. A) Coronal sections of the initially flat tissue of the hippocampus folding medially during development, forming the hippocampal sulcus (indicated by arrow). B) Fully developed hippocampus seen from above, showing the longitudinal curvature in the head and tail and anterior digitations. Both images adapted with permission from (Duvernoy *et al.*, 2013) <permission pending>.

1.2 Hippocampal ontogeny and folding about the 'dark band'

During development, the hippocampus originates from a single flat tissue, which in addition to its long-axis curvature, also folds medially upon itself while differentiating into the various subfields (Duvernoy *et al.*, 2013; Williams, 1995; Smith, 1897)(Figure 1A). This developmental characteristic has several interesting consequences for the structure of the adult hippocampus: all subfields makeup adjacent segments of a contiguous tissue segment (though the dentate gyrus makes up a distinct tissue but keeps a consistent position at the distal edge of the CA fields). The CA fields wrap around the innermost subfield - the dentate gyrus - forming a 'C' shape which can be seen in coronal sections throughout the hippocampal body, denoted here as the proximal-distal axis. Thus there are consistently preserved and contiguous spatial relationships between the subfields after this folding is taken into account. The sulcus, or 'crease' around which this folding occurs can be visualized in histology as the hippocampal sulcus, or in MRI as the 'dark

band' - an image feature related to high myelin laminae in the tissue surrounding this sulcus (Kerchner *et al.*, 2010; Thomas *et al.*, 2008, and others), and perhaps to the presence of non-penetrating blood vessels in the sulcus. Since the dark band is adjacent to all hippocampal subfields throughout the entire length of the hippocampus, it can serve as a feature to aid in the computational unfolding of the hippocampus. By unfolding the hippocampus along both the longitudinal and proximal-distal axes, the complex spatial arrangement of subfields in three dimensions can be considerably simplified.

1.3 Computational unfolding with Laplace's equation

In the neocortex, 3D computational tools such as Laplace's equation have been used to precisely and flexibly calculate neocortical thickness (e.g. Jones *et al.*, 2000; Sowell *et al.*, 2004). In principle, the Laplace equation, $\nabla^2\varphi = 0$, defines a potential field (φ) whose values change based on their distance from two boundary surfaces. The solution is twice-differentiable ($\nabla^2 = 0$), which guarantees a level of smoothness that is appropriate for anatomy. In studies of neocortical thickness these boundaries are the white matter and pial surface, while the potential field spans the neocortical grey matter. Thickness is then computed by generating streamlines across the resulting potential field gradient.

We reasoned that Laplace's equation may also be used for unfolding of hippocampal grey matter, not only to determine thickness along the laminar dimension, as above, but also to compute potential field gradients along the longitudinal and proximal-distal dimensions. To do so, it is critical to employ multiple sets of boundary conditions, sometimes referred to as 'source' and 'sink'. For example, unfolding along the longitudinal dimension makes use of anatomically motivated boundaries at the anterior (source) and posterior (sink) ends of the hippocampus. The potential field in between is defined over all grey matter, and increases smoothly from source to sink. We thus solved Laplace's for three different equations, $\nabla^2\varphi_{longitudinal} = 0$, $\nabla^2\varphi_{proximal\text{-}distal} = 0$, $\nabla^2\varphi_{laminar} = 0$, to determine a different potential field for each hippocampal dimension. The domain was identical for each, as the hippocampal gray matter, but the boundary conditions were distinct in each, defined as anatomical landmarks along at the edges of the hippocampal tissue (section 2.6).

1.4 Goal of the current study

The current study aimed to develop a method for investigating hippocampal structure that accounts for the known ontological folding, long-axis and uncal curvature, digitations, and inter-individual variability found

in hippocampal morphology. We employ a time-efficient tracing and dilation technique for detecting the hippocampal 'dark band' and surrounding grey matter, and we then use Laplace's equation to 'unfold' hippocampal grey matter. We demonstrate the utility of this technique by using it to map the trajectories of the subfields of the hippocampus into this unfolded coordinate space. We evaluate how much variability is accounted for in the folding of the hippocampus by examining how subfield boundaries are aligned in the intrinsic, unfolded coordinate space, and demonstrate an atlas-based segmentation of the subfields that does not utilize 3D deformable image registration. We also examined the histological validity of this approach using a single dataset with corresponding surgically-resected tissue sample and ground-truth subfield labels. Finally, we demonstrate the utility of this unfolding for mapping out other quantitative properties of hippocampal tissue in a standardized, 'unfolded coordinate space'.

2 Methods

2.1 Study participants

For MRI data acquisition, healthy participants were recruited from Western University, London, Canada (n = 12; 6 females; ages 20-35, mean age 27.6). This study was conducted with Western's Human Research Ethics Board approval, and informed consent was collected from each participant prior to participation.

2.2 MRI acquisition

Imaging was performed using a 7T neuroimaging optimized MRI scanner (Agilent, Santa Clara, CA, USA/ Siemens, Erlangen, Germany) employing a 23-channel transmit-receive head coil array constructed in-house. Four T2-weighted turbo spin echo (TSE) 3D (3D sagittal, matrix: 260x366, 266 slices, 0.6mm^3 isotropic, ~8.5 mins per scan) images were acquired from each participant. By using isotropic voxels, we are able to capture small features such as the hippocampal dark band in high detail, even when it is parallel to the orientation of image acquisition (which is often the case in the hippocampal head and tail). A T1-weighted MPRAGE (3D sagittal, matrix: 256x512, 230 slices, 0.75mm^3 isotropic) image was also collected.

2.3 Preprocessing

All scans were resampled to coronal oblique as follows: the first T2-weighted image (scan 1) was upsampled to 0.3mm^3 isovoxels using cubic spline interpolation, then scans 2, 3, and 4 were rigidly registered it using FSL FLIRT registration (Jenkinson, 2002; Tofts, 2005). All four scans were then averaged together to

produce a single, 0.3mm^3 isovoxel, high-contrast volume. This volume was then reoriented to an oblique orientation, with coronal slices perpendicular to the long axis of the hippocampus, by rigid registration to an average template in coronal oblique orientation. T1-weighted scans were registered to this high-contrast coronal oblique T2-weighted volume using rigid registration as above.

2.4 Detection and labelling of the hippocampal 'dark band' and grey matter

Under our isotropic MR acquisition protocol, the hippocampal dark band was visible in the entire longitudinal extent of the hippocampus, including the digitations and uncus of the hippocampal head. Exemplary slices from the hippocampal head and body and a 3D model reconstruction can be seen in Figure 2A. All manual tracing was performed in ITK-SNAP 3.4 (Yushkevich *et al.*, 2006), and the built-in 'Snake' tool was also used to facilitate tracing. The detailed protocol for tracing, 'feathering', dilation, and manual adjustments can be found in Supplementary Materials.

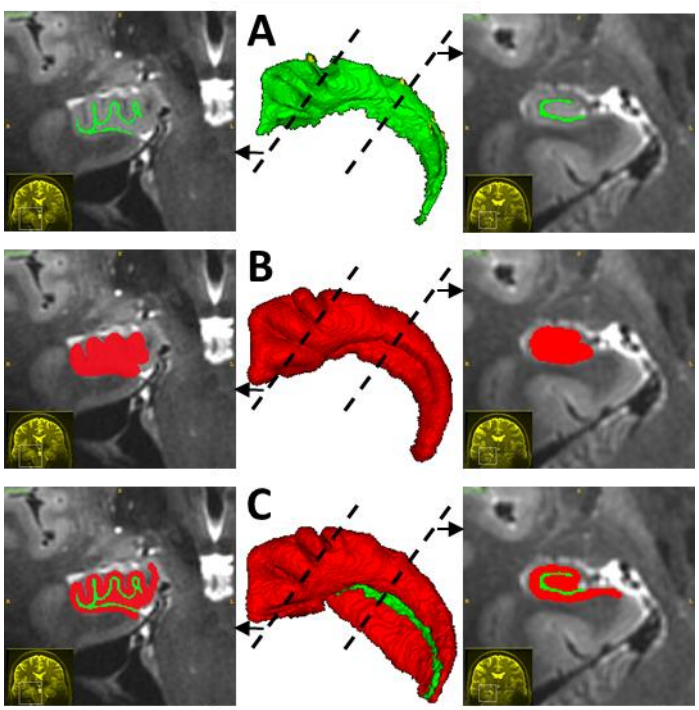

Figure 2 <single column width, coloured>. Illustration of dark band (green) and hippocampal grey matter (red) labelling. A) 3D model of the dark band label in the center, with example coronal slices from the head and body on the sides, at the positions indicated by the dotted lines. B) Same views as above, but depicting the dark band label after spherical dilation. C) Same views as above showing the combined dark band label and grey matter label, after manual adjustments to the grey matter label.

Much of the morphology of the hippocampus is systematically related to the dark band (e.g. size and position, number and locations of digitations; curvature of the uncus and tail; see Figure 2). The various subfields of the hippocampus surround the hippocampal dark band, and thus we made use of this proximity to initialize grey matter segmentation with the dark band segmentation. We segmented the gray matter of the hippocampus by an initial active contour evolution of the dark band, followed by manual correction. We used ITK-SNAP's Snake tool (Yushkevich *et al.*, 2006), which evolves a seed region in 3D to fill a structure of interest. In our case, we initialized the evolution using the dark band and first applied no constraints on the evolution, resulting in uniform, spherical dilation. The amount of dilation was determined by visually inspecting whether the outer borders of hippocampal grey matter had been reached, and varied slightly between traces depending on the available image information. Evolution constrained by edge attraction (with parameters defined by the user based on image quality) and manual adjustments were then applied. The subiculum, a medial and less folded extension of hippocampal grey matter, has no dark band border and, thus, had to be labelled manually. This was also the case in the most medial, vertical component of the uncus where the dark band was often not visible. Further manual adjustments included the removal of grey matter label from the CSF on the medial side of the dentate gyrus, and minor adjustments throughout to ensure all grey matter was labelled as such. Errors in manual segmentation can produce distortions on the next step of hippocampal grey matter unfolding, so the unfolding results of each hippocampus were examined manual segmenters to ensure their labelling followed the rules outlined in Supplementary Materials.

To assess how reliably the dark band could be segmented in our high-resolution images, we repeated the segmentation by an additional trained rater, and calculated the spatial overlap between these segmentations using the Dice similarity index (DSI). DSI represents the proportion of overlapping voxels in two segmentation labels over the mean number of voxels per label, and so it can vary from 0 to 1, with values close to 1 denoting high overlap (Dice, 1945).

2.5 Manual segmentation

Before unfolding of hippocampal grey matter, we performed manual segmentation of this tissue into subfields in a set of 10 hippocampi (5 participants x2 hemispheres) with varying numbers of digitations and varying curvature in the uncus. This was done by carefully matching coronal views in our MR images with the closest corresponding histological segmentations in the hippocampal head provided by Ding & Van Hoesen (2015). In the hippocampal body and tail, segmentations were performed based on the descriptions of Duvernoy *et al.* (2013). Note that it was not our intention to develop a manual segmentation protocol in

this paper, we simply aimed to determine whether the trajectories of the hippocampal subfields in our unfolded coordinate space could be captured in a way that respects the recently elucidated complexity in the hippocampal head.

2.6 Unfolding of hippocampal grey matter

The critical feature of our unfolding technique is the selection of anatomically motivated boundaries to be used in the Laplace equation. Appropriate landmarks were chosen at the termini of each dimension of interest: longitudinal, proximal-distal, and laminar (as below). An iterative finite-differences approach was then used to obtain the solution for each pair of boundaries, by using a 26-neighbour average to compute the updated potential field, and terminating when the potential field change is below a specified threshold (sum of changes < 0.001% of total volume). It is important that the dark band voxels are not included in the gray-matter domain of Laplace's equation, since this effectively provides a barrier so that the streamlines follow a geodesic path along the hippocampus and do not introduce short-circuits. Solving of the Laplace equations was performed in MATLAB (code available at https://github.com/jordandekraker/HippUnfolding).

Longitudinal dimension boundaries

Each of the subfields follows the curvature of the uncus and therefore has its natural terminus not in the tip (most anterior portion) of the hippocampus but rather in the more medial and posterior uncus (specifically, the vertical component of the uncus) (Ding & Van Hoesen, 2015). Hippocampal grey matter in this area borders the grey matter of the amygdala, making up an area that is typically referred to the hippocampal-amygdalar transition area (HATA). At the tail of the hippocampus, a structure called indusium griseum (which is actually an extension of the dentate gyrus) extends medially and posteriorly from the hippocampus and then curves upward and anteriorly along the midline of the brain before merging with the cingulate cortex. The HATA and indusium griseum thus make up two visible structures which correspond to the natural anterior and posterior termini of each of the hippocampal subfields. We manually traced these structures only where they border hippocampal grey matter, and used them as source and sink regions in Laplace's equation (see Figure 3A for illustration).

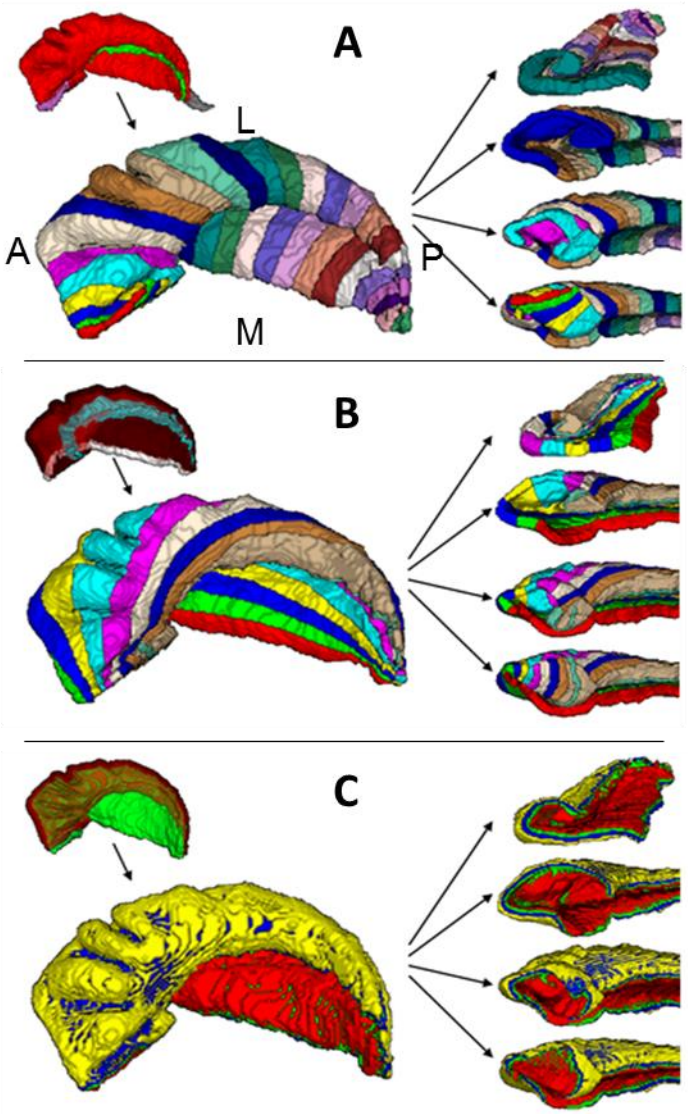

Figure 3 <single column width, coloured>. Illustration of Laplacian unfolding along the longitudinal, proximal-distal, and laminar dimensions in A), B), and C), respectively. The upper left inset image in A) shows a 3D model of the hippocampal dark band (green) and grey matter (red) labels, with the HATA (pink) and indusium griseum (grey) to be used as boundaries for Laplace's equation. The lower left image in A) shows arbitrarily coloured bins within the resulting potential field gradient. To the right is the same model as the lower left, but showing cross sections from the body (top) and head (lower three), depicting in particular the uncus (lower two) and vertical component of the uncus (bottom). B) and C) show the same views of the same hippocampus, but using the inner dentate gyrus (turquoise) and medial temporal lobe cortex border (white), and the dark band (seen in green under semi-transparent red grey matter) and outer hippocampal borders as boundaries for Laplace's equation for the proximal-distal and laminar dimensions, respectively.

Proximal-distal dimension boundaries

We defined the proximal border as the point at which the subiculum, the most proximal subfield, contacts the grey matter of neighbouring medial-temporal lobe neocortex (see Supplementary Materials for details).

To index the full extent of hippocampal grey matter, the distal border of hippocampal grey matter can be defined as the granule cell layer of the dentate gyrus (i.e. the part of dentate gyrus which most closely borders the dark band). We employed a custom approach to detect this tissue: within each previously computed longitudinal bin we applied volumetric fast marching (Sethian, 1999) along hippocampal grey matter starting at the border with surrounding temporal lobe cortex, and approximated the dentate gyrus as being the most distal 12% of this distance (determined experimentally). To index only the innermost granule cell layer of this tissue, we dilated the dark band by a single voxel (8 nearest neighbours) over this rough dentate gyrus approximation. The result included only the most distal portions of the dentate gyrus, corresponding roughly to the granule cell layer.

An additional challenge in the proximal-distal unfolding of the hippocampus lies in the vertical component of the uncus. Here, hippocampal grey matter doesn't follow the classic folded 'C' shape as the rest of the hippocampus and instead flattens out (Figure 3 bottom right). The dentate gyrus persists on the medial edge of this region, but is not separated by the other subfields by a visible dark band with the current image resolution. We thus defined the dentate gyrus' location manually for this region (Figure 3B).

Laminar dimension boundaries

We defined the sink for Laplace's equation as the outermost surface of the hippocampus, and the source as the hippocampal dark band. However, as mentioned in section 2.1, the subiculum and vertical component of the uncus do not border the hippocampal dark band, and so they were artificially extended over these regions. For the subiculum, this was done computationally by dilating the dark band label along the surface of the subiculum until the most medial point was reached in each coronal slice. For the vertical component of the uncus this label was created manually. These artificially extended labels were used in as the source in Laplace's equation (Figure 3C).

2.7 Subfield borders in unfolded coordinate space

The longitudinal and proximal-distal potential field gradients together make up a 2D coordinate system that can be used for indexing columns of hippocampal grey matter. Using this 'unfolded coordinate space', we can index the location of each subfield border. We used the manual subfield segmentations performed on 10 hippocampi (see section 2.5) to generate a subfield atlas in the unfolded coordinate space. That is, for each manually segmented hippocampus, we found the longitudinal and proximal-distal coordinates which

correspond to each of the subfield borders. We then averaged these borders together at each longitudinal point, and plotted the labelled data in the 2D unfolded coordinate space (see Figure 6). The unfolded atlas was then used to automatically segment subfields in each subject's hippocampus.

We assessed the overlap of the 10 manually segmented hippocampi to their unfolded group-average border segmented counterparts using Dice Similarity Indices. To avoid bias, we used a leave-one-out approach where a given participant's manual segmentations (both left and right) were not included in unfolded group-averaged borders.

2.8 Histological validation

One temporal lobe epilepsy patient with left mesial temporal sclerosis (age 34; male) underwent preoperative 7T scanning and then went on to receive a left anterior temporal lobectomy, with amygdalo-hippocampectomy, as part of their standard of care. The surgical tissue underwent a standardized protocol involving overnight scanning in a ultra-high field *ex vivo* 9.4T MRI, agar embedding, and cutting into blocks 4.4mm apart for paraffin embedding and histological sectioning. Staining with H&E, Neu-N, GFAP, and Luxol fast blue was performed, and slides were digitized at 0.5 micron/pixel resolution. The subfields were manually annotated on the Neu-N histology images, with criteria outlined in Ding & Van Hoesen, using the Aperio ImageScope software. We employed our previously developed and validated pipeline for MRI and histology registration (Goubran *et al.*, 2015, 2013) to perform direct validation of 7T hippocampal subfield segmentation against ground-truth histological sections. The histology-MRI image registration procedure involved iterative 2D-3D deformable registration of downsampled (100 micron/voxel) histology slides to the reference 9.4T tissue MRI, along with 3D deformable landmark-based registration of the 7T MRI to the 9.4T MRI. Segmentation labels as well as the proximal-distal gradient from the *in vivo* 7T images were then propagated to this aligned histology space for direct comparison to the histological ground truth.

2.9 Quantitative unfolded tissue properties

Properties such as intra-cortical myelin content and cortical thickness have been shown to be useful for parcellation of the neocortex into functional subregions (e.g. Glasser *et al.*, 2014; Glasser and Van Essen, 2011). The ratio of T1-weighted over T2-weighted values produces a map that is correlated with quantitative R1, and is used as a surrogate measure of intra-cortical myelin (Glasser and Van Essen, 2011). We estimated intra-cortical myelin in this way, and estimated cortical thickness by fitting streamlines to the laminar

potential field gradients of all hippocampi. We then plotted these values across unfolded coordinate space. To avoid confounds from partial voluming, we mapped the myelin contents of hippocampal tissue from only the middle 25-75%, as determined by our laminar Laplacian field, corresponding to approximately 2 voxels at our resolution, but similar results were obtained when the superficial and deep laminae were included as well. To illustrate how these values map onto the native 3D space of the hippocampus, we generated 3D hippocampal models with surface colouring that corresponds to the underlying myelin estimates from the group average in two hippocampi (one highly digitated and one less digitated exemplar).

3 Results and discussion

3.1 Detection and labelling of the hippocampal 'dark band' and grey matter

To assess reliability, inter-rater DSI was calculated for dark band and grey matter labels. Note that DSI tends to be lower for thin structures at higher resolutions because of the high surface area to volume ratio. DSI revealed good spatial overlap in both the dark band (0.72±0.03 right; 0.70±0.04 left) and hippocampal grey matter (0.84±0.01 right 0.81±0.02 left). Thus our dataset contained sufficient contrast to consistently detect and label the hippocampal dark band and grey matter based on the visual features described in Supplementary Materials.

3.2 Unfolding of hippocampal grey matter

Our approach to subfield segmentation and broader understanding of the structure of the hippocampus *in vivo* was to unfold this hippocampal grey matter tissue along its longitudinal and proximal-distal axes. The following observations were made during the process of computationally unfolding hippocampal grey matter about the dark band using Laplace's equation:

- In the longitudinal unfolding, a cross-section of hippocampal grey matter at an equipotential point in the hippocampal body (e.g. Figure 3A, top right) reveals the same classic 'C' shaped orientation of grey matter as in coronal slices from histology and in extant MRI tracing protocols. Unlike in the coronal or other views, however, cross-sections at equipotential points in the hippocampal head in our unfolding reveal the same 'C' shaped orientations of subfields (e.g. Figure 3A, middle right).
- In the most medial, or the 'vertical', component of the uncus, the 'C' shape of hippocampal grey matter flattens out to form a line (e.g. Figure 3A, lower right). Here, the dentate gyrus passes most medially around the other subfields before extending upwards and reaching the vertical component of

the uncus (Ding & Van Hoesen, 2015), a feature that is accounted for in our unfolding by the manual placement of the 'sink' in the proximal-distal unfolding of hippocampal grey matter (Figure 3A).

- In the proximal-distal unfolding, the more proximal regions of hippocampal grey matter wrap around the absolute anterior of the hippocampus, moving from the inferior to superior side, as in the descriptions of the subiculum by Ding & Van Hoesen (2015) (Figure 3B green, blue, and yellow bins)
- The 'sink' used for proximal-distal unfolding captures most of what corresponds to the granule cell layer of the dentate gyrus in histological sections, except the very most medial parts of this cell layer which often do not border the hippocampal dark band (Duvernoy *et al.*, 2013) and so are not captured by our 'sink' label (see Figure 3B, top right). Thus caution should be used if attempting to index the granule cell layer of the dentate gyrus using this method.
- The laminae of the dentate gyrus actually sit perpendicular to those of the other subfields (Duvernoy *et al.*, 2013). This is not respected by our laminar unfolding and instead most of the dentate gyrus is treated as being deep laminae (e.g. Figure 3C). Thus caution should be used if attempting to index the laminae of the dentate gyrus.

Other advantages to this 'unfolded' space include the fact that all distances are relative to the full size of the hippocampus, and can thus be applied across a range of hippocampal sizes and morphologies. With some adaptation of landmarks used as boundaries in the Laplace equation (i.e. source and sink), this protocol may also be applied to abnormally developed hippocampi or even those from other mammalian species. Despite gross differences in position and morphology, the properties of hippocampal tissue can still be mapped out in analogous 'unfolded' space.

3.3 Subfield borders in unfolded coordinate space

The subfields projected into unfolded coordinate space are shown in Figure 4. As predicted, the same proximal-distal arrangement of subfields was found throughout the entire hippocampus in unfolded coordinate space, including the hippocampal head (Figure 4). Variability was low for all borders (i.e. low SEM) considering the gross morphological differences in native 3D space, and no subfields crossed over each other either in the group average or in any given unfolded segmentation example. This qualitative observation agrees with our predictions based on the ontogeny and descriptions of the fully developed hippocampus (Section 1.2).

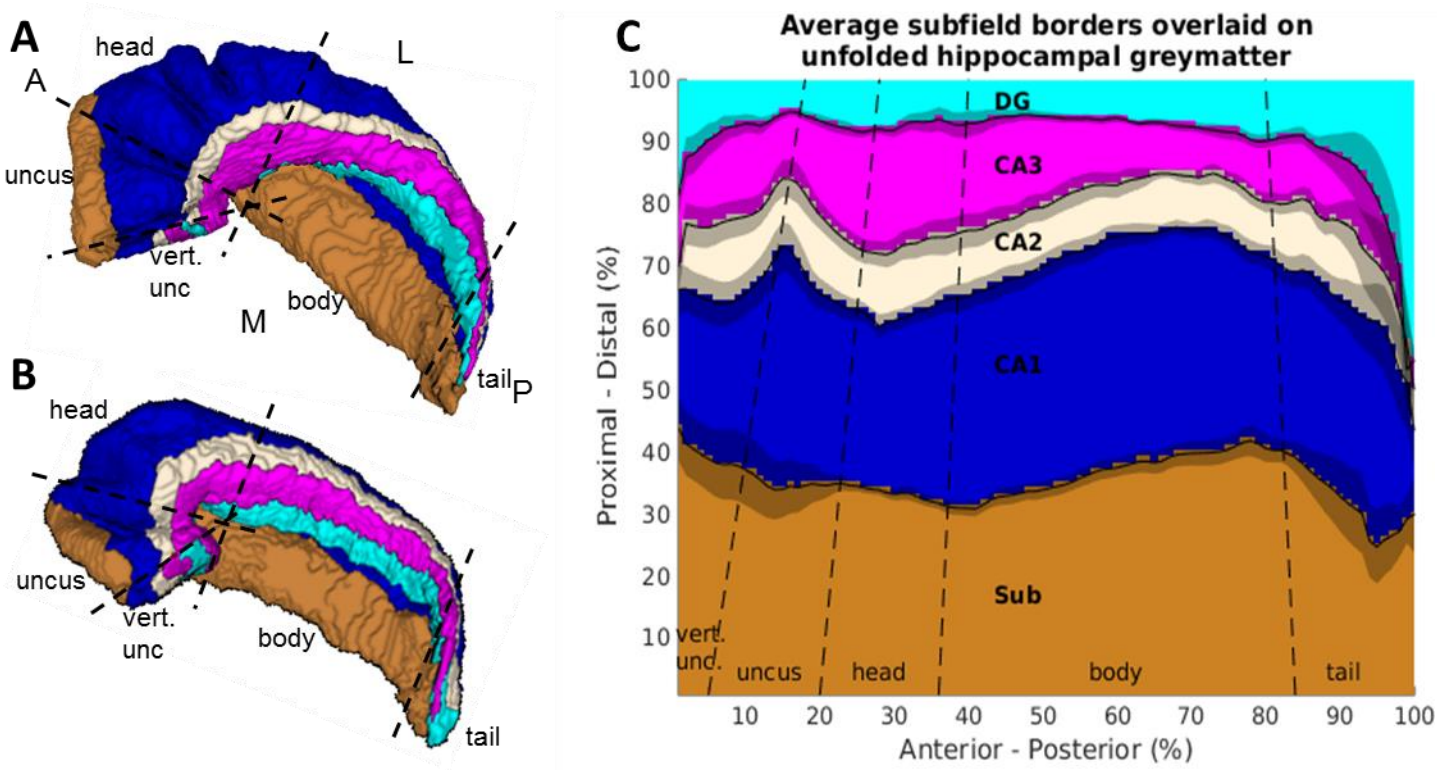

Figure 4 <double column width, coloured>. Hippocampal segmentations in unfolded coordinate space. A) Example of a manual subfield segmentations based on (Ding & Van Hoesen, 2015). B) Same as A), but showing an exemplar with less digitatations and medial curvature. C) Flattened out or 'unfolded' hippocampal grey matter, with subfield label identity determined at each longitudinal and proximal-distal coordinate from the manual segmentations (winner-takes-all over the sample). The shaded areas indicate standard error of the mean for each subfield boundary location across the sample of manual segmentations. Dotted lines approximately indicate commonly used boundaries between the hippocampal head, body, and tail, with head further subdivided into uncus and vertical component of the uncus.

The fact that the SEM of the average unfolded borders was relatively low (i.e. accounts for a relatively small proportion of the area of each subfield) was surprising given the large inter-individual variability of subfield locations in native space (Ding & Van Hoesen, 2015). This suggests that much of the variability in native space is due to differential curvature and folding of hippocampal tissue in development, rather than differences in the cytoarchitectural differentiation within this tissue. The borders shown in Figure 4 were applied to our entire sample of unfolded hippocampi (12 left/12 right). This atlas will be made freely available online <Open Science Framework (http://osf.io) repository pending>.

Comparing unfolded group-average segmented hippocampi to their manually labelled counterparts revealed a high degree of spatial overlap (Figure 5). As expected, lowest DSI was seen for the smallest subfields-CA2 and CA3. Combining these two labels lead to improvements, making spatial overlap for these subfields

similar to that seen in extant protocols, and spatial overlap for the other subfields was comparable or even higher than current manual segmentation protocols (e.g. Winterburn *et al.*, 2013 (3T); Wisse *et al.*, 2011 (7T); Yushkevich *et al.*, 2009 (9.4T *ex vivo*)). High spatial overlap provides additional evidence that the intrinsic alignment gained by performing our unfolding is able to map subfield boundaries across subjects. Note that this is accomplished without any inter-subject non-linear registration, which would be ill-posed when number of digitations differ; instead simply utilizes the intrinsic geometry of each hippocampus. Note also that as seen in Figure 7C, there are discrepancies between manual segmentations and intracortical myelin not seen in the unfolded group-average segmentations. Thus differences in overlap between manual and unfolded group-average segmentations may be partially due to errors in manual segmentations that average out in the unfolded border segmentations.

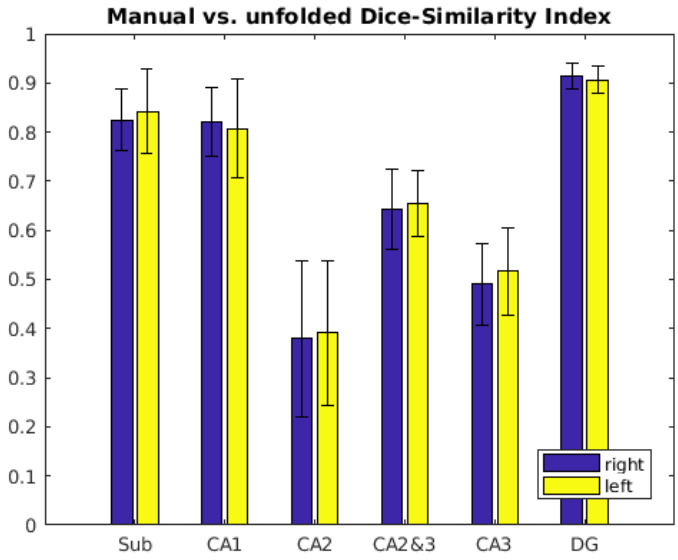

Figure 5 <single column width, coloured>. Spatial overlap in Dice Similarity Index (DSI) between leave-one-out unfolded group-average subfield segmentations and their manually segmented counterparts. The leave-one-out technique was performed such that borders from one participant's left and right hippocampi were not included in the averaged borders that informed unfolded segmentation of that participant's hippocampi.

3.4 Histological validation

Segmentation on *in vivo* 7T data from one surgical patient are compared to the same patient's *ex-vivo* resected and histologically stained hippocampus in Figure 6. Atrophy and cell loss in area CA1, CA3, and the dentate gyrus, with relative sparing of CA2, can be seen in the epileptogenic tissue (Figure 6, far left); these findings describe classical hippocampal sclerosis (Blümcke *et al.*, 2007). Note also that this patient

shows only two clear digitations in the hippocampal head, which were not well captured in the *in-vivo* labelling of grey matter tissue. *In-vivo* segmentations showed some other misalignment of both grey matter and dark band labels, which can be seen in areas where neurons can be seen in the histology without being obscured by grey matter labels. This likely reflects imperfect alignment between the *in-vivo* scan and *ex-vivo* histology, but may also be due to poor image quality in this patient making it difficult to correctly label hippocampal grey matter and dark band.

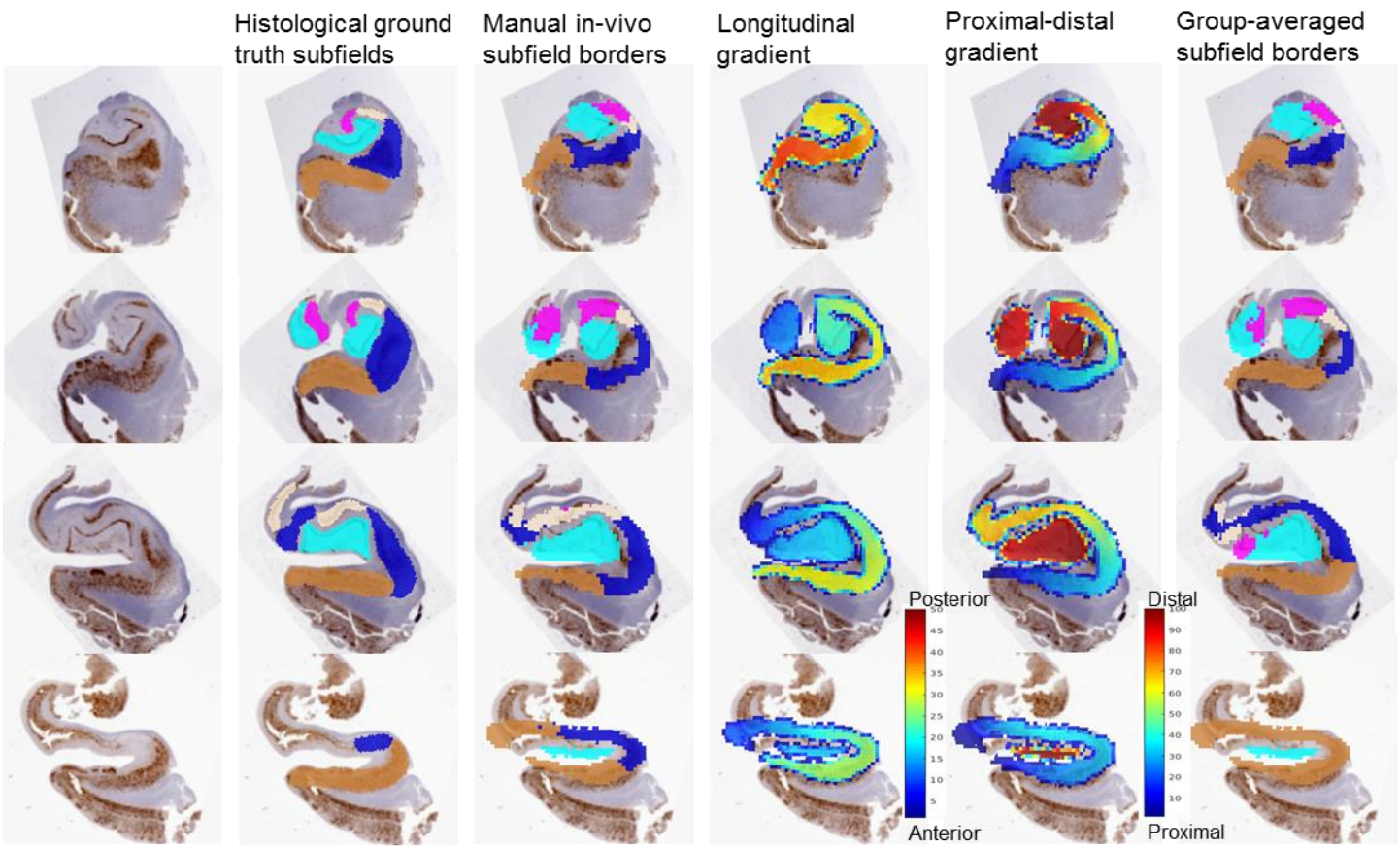

Figure 6 <double column width, coloured>. NeuN stain of resected hippocampal tissue with comparison of histologically segmented hippocampal subfields to *in-vivo* subfield labels and unfolding Laplace gradients in the same individual. Slices move from posterior (hippocampal body) to anterior through the hippocampal head, and are separated by 4.4mm. The proximal-distal and longitudinal gradients are surrounded by low color scaled voxels because of their interpolation when transforming to the histological space. The subfield colour scheme is as follows: cyan = dentate gyrus; pink = CA3; white = CA2; blue = CA1; brown = subiculum.

Some errors can be seen between the *in-vivo* manual subfield segmentation and the histological ground truth. This could be due to misalignment, tissue atrophy, and poorer image quality, as mentioned above, but several key features are still present. Particularly, CA2 passes into, then out, then back into plane in row 3,

and both dentate gyrus and CA3 are seen in the uncus in row 2. Because these borders are curved medially in the head, they are difficult to capture in coronal slices alone and will vary drastically depending on the exact position of the slice. Thus, using isotropic voxels in image acquisition and labelling protocols that can leverage 3D cues provides a potential for greater precision and validity.

The longitudinal and proximal-distal gradient together make up our two-dimensional unfolded coordinate space, which we examine here with respect to histology. The longitudinal gradient changes between coronal slices, as expected when moving from posterior to anterior, but also changes within each slice. This is because the anterior point is located in the most medial, vertical component of the uncus where each of the subfields has its natural terminus, rather than the absolute anterior of the hippocampus. Thus the longitudinal gradient here shows how any given coronal slice is out-of-plane with respect to the medial curvature of the uncus. The proximal-distal gradient identifies a set of potential subfield borders, which can also be adjusted depending on anterior-posterior extent. In rows 2 this gradient can be seen to increase and then decrease as the gradient passes into and then out of the plane of view, similar to what is seen in the histological ground truth images. We used this gradient in combination with the longitudinal gradient to apply group-averaged subfield borders to this participant's unfolded hippocampal space. This segmentation suffers from many of the same issues as the fully manual segmentation, but as in the manual segmentation many of the key features of the hippocampal head are retained, such as the passing into and out of plane for CA2 and the presence of CA3 in the uncus (rows 2 and 3, respectively). However, both in the unfolded group-average segmentation and in the fully manual segmentation, each of the *in-vivo* segmentation borders should be shifted more distally in rows 1 and 2, and more proximally in the unfolded group-average segmentation in rows 3 and 4. This resulted in no CA1 label in row 4 of the unfolded group-average segmentation. These errors may arise because of tissue atrophy and poor grey matter labelling in this participant as compared to healthy controls. Such factors may make manual segmentation based on Ding & Van Hoesen (2015)'s descriptions, or using the borders established in healthy control participants less appropriate for this patient. Nevertheless, in addition to demonstrating how our unfolded coordinate space maps onto histology, this application illustrates how segmentations in unfolded coordinate space, in this case using borders determined in a group of healthy participants, are able to capture critical structural complexities of the hippocampal head.

Note that the current unfolding method is not bound to use of this particular segmentation protocol and borders from other segmentation protocols can also be mapped out in unfolded coordinate space and applied

to large sets of unfolded hippocampi. In the present study we focused primarily on borders defined based on Ding & Van Hoesen's recent histological descriptions (2015), but in principle any borders can be indexed in this way, including those that may emerge as international consensus is reached on the precise subfield border definitions (see Wisse *et al.*, 2017).

3.5 Quantitative unfolded tissue properties

Unfolding provides a way to view grey matter properties across the entire extent of the hippocampus in a single 2D view. This unfolded view can obviate patterns that are not apparent when limited to single slices in native, 3D space. Here, we mapped intracortical myelin and cortical thickness (Figure 7), but additional properties including those used by Glasser *et al.*, (2016) can be mapped in this way as well.

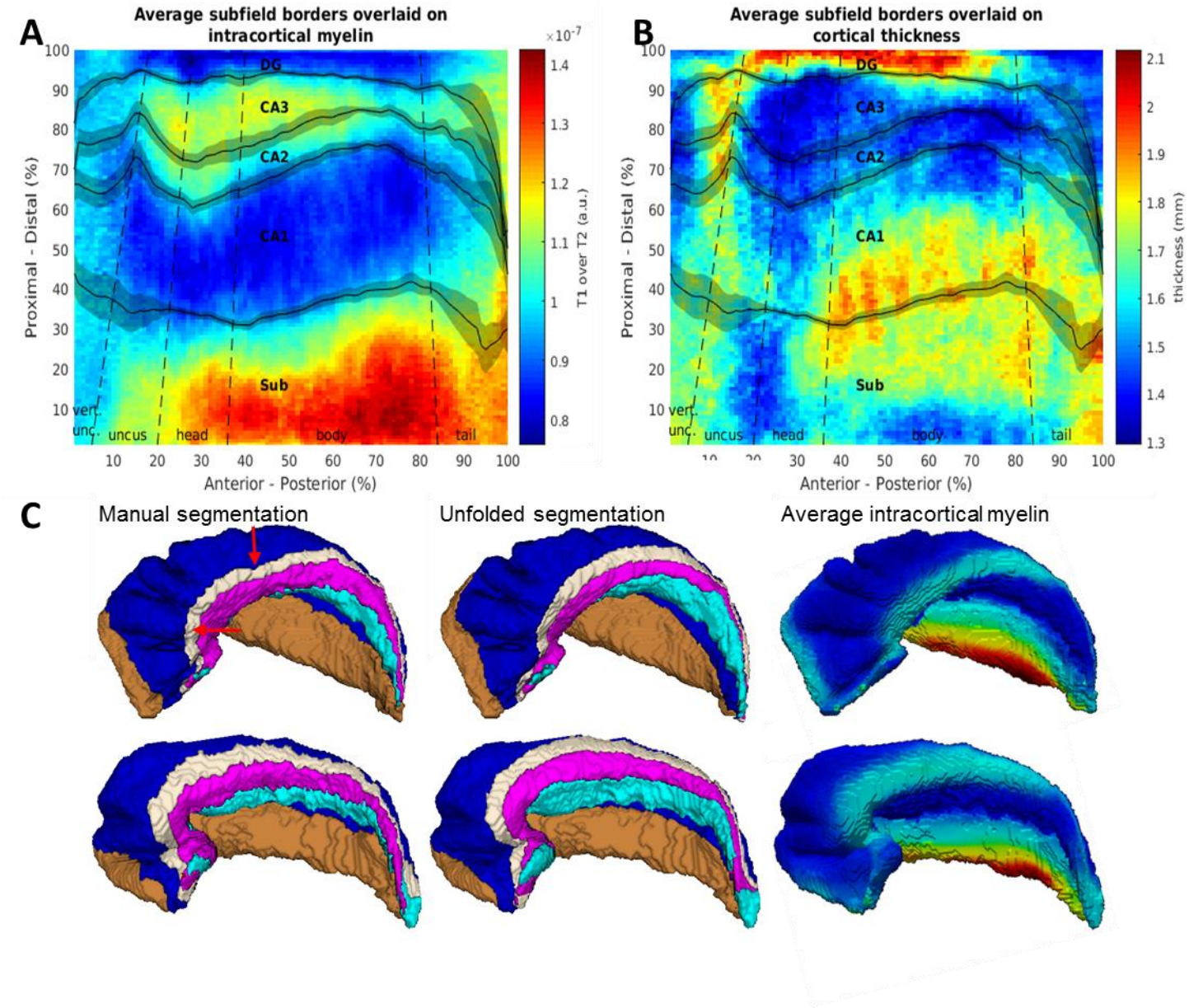

Figure 7 <double column width, coloured>. Quantitative mapping in unfolded coordinate space compared to subfield borders. A) Average intracortical myelin estimates (T1 over T2 MR intensities; arbitrary units). B) Average cortical thickness. Both A) and B) have average subfield borders overlaid. Note that in the dentate gyrus, thickness estimates are actually perpendicular to the true laminar structure (see section 3.2). C) Manual and unfolded subfield segmentations compared to intracortical myelin in highly digitated (top) and less digitated (bottom) example hippocampal models. Average intracortical myelin is mapped to the surface models of these hippocampi for easier comparison. Red arrows indicate points of interest (see text).

Intracortical myelin estimates appear to closely correspond to the average subfield borders used in our demonstration of subfield segmentations (Figure 7A). The subiculum and areas CA2 and CA3 appear to have greater myelin content than CA1 and the dentate gyrus, with the proximal part of the subicular complex

showing greatest values. Though speculative, we suggest that this could reflect contributions of the perforant path, which 'perforates' the subiculum, elevating myelin estimates because of the presence of white matter tracts. In area CA3, dense recurrent collaterals might contribute to elevated myelin estimates. An alternative explanation is that increased vasculature, which would appear dark in T2-weighted images, contributes to this contrast. Support for this explanation comes from the observation that area CA2 is the most highly vascularized subfield in humans (Duvernoy *et al.*, 2013). These findings also agree with those of Abraham *et al.* (2012) who examined intracortical myelin in histological samples, and Marques and Guetter (2013) who found similar differences in R1 MR intensities between the subfields. Currently, no extant subfield labelling protocols explicitly leverage these differences in MR intensities, perhaps due to reduced contrast seen in a single coronal slices from a given participant. By aligning across multiple participants and examining the entire length of the hippocampus, the intracortical myelin estimates reveal sharp changes in contrast that closely match our predicted subfield borders. Comparing both, manual and unfolded group-average segmentations to intracortical myelin (Figure 7C), we see that there are some discrepancies between border locations and intracortical myelin, particularly in the manual segmentations shown here. For example, in the upper row we see that CA2 in the body of the hippocampus dips more distally in the manual segmentation than in the unfolded group-average segmentation or the average intracortical myelin, and more proximally in the hippocampal head (see red arrows). This is likely due to imperfect alignment between coronal slices in MRI with histological reference slices from Ding & Van Hoesen (2015) and Duvernoy *et al.* (2013). Furthermore, the borders seen in manual segmentations are more jagged than the unfolded borders or intracortical myelin changes. These issues may reflect principal challenges related to the reliability and feasibility of manual segmentation protocols, which fall beyond the scope of the current paper. Nevertheless, the fact that these discrepancies largely average out in a sample of unfolded hippocampi, while still respecting differences in morphology, further highlight the capability of the approach taken here.

Cortical thickness was also calculated using Laplacian streamlines and mapped in unfolded coordinate space (Figure 7B), but these differences do not appear to correspond to the subfield borders. Note that thickness in the dentate gyrus was actually calculated perpendicular to the true laminae of the dentate gyrus because of the different orientation of tissue (see Section 3.2). Thus thickness in this region should not be considered to reflect true laminar structure. Overall, these results are similar to thickness measures obtained within the hippocampus by Yushkevich *et al.* (2011), who found that thickness was highest between subiculum and CA1 and lowest in CA3 both in healthy and mild cognitive impairment patients. However, these results differ from Burggren *et al.* (2008), who found that thickness was high in CA3/dentate gyrus, particularly in

the anterior hippocampus. This may be because their study performed hippocampal unfolding but did not account for the digitations in the hippocampal head, which could have led to overestimation of the thicknesses.

Cues such as intra-cortical myelin, thickness, or others may be useful in generating subject-specific subfield borders in the future. The unfolding of hippocampal grey matter accounts for much of the inter-individual variability due to differences ontological folding, but variability due to the presence of disease, as in the resected tissue presented here, might create additional variability in unfolded subfield locations and sizes. This presents a significant challenge when trying to apply unfolded group-average borders, as well as for manual or automated segmentation protocols which rely on geometric rules and structural landmarks (which could themselves introduce additional variability). Thus the use of additional MR intensity information, possibly across multiple acquisition modalities, could guide a deformation of the average subfield border locations in order to obtain a better fit of an individual's unfolded hippocampal space. This possibility can be explored in future follow-up work.

3.6 Hippocampal unfolding in the context of extant literature

One possible source of the recent controversy over hippocampal subfield borders relates to constraints that in order to be reliable, a coronal slice segmentation protocol has to make use of heuristics such as geometric rules with reference to visible intra- or extra-hippocampal landmarks. For these rules to be applicable across different hippocampal morphologies and MR image qualities, some level of simplification is necessary, reducing accuracy and precision. Given the large number of possible border locations, the unfolded coordinate system presented here has the inherent feature of allowing for increased precision, even across hippocampi with varied morphologies because it respects critical structural features of the hippocampal head without reliance on the heuristics mentioned. Thus, although we do not wish to present the specific subfield borders used here as an alternative to the efforts towards international harmonization by the Hippocampal Subfields Group, we hope that these efforts will include the structural considerations discussed in the current paper, and may also lead to exploration of methodologies other than manual segmentation. Furthermore, we anticipate that, once international consensus is reached, the resulting subfield borders can be applied using the unfolded coordinate system presented here, and complemented by further characterization of inter-individual differences that can be captured with the present methodology. Given the increasing prevalence of high-resolution data in which the hippocampal dark band can be seen throughout the length of the hippocampus, this appears to be a particularly promising avenue.

It is worth noting that the current protocol is not the first to consider hippocampal unfolding, and that similar proximal-distal unfolding has been carried out in medial-temporal lobe structures, including hippocampal subfields, in prior work as well. Several studies reported by Bookheimer and colleagues have implemented a technique to segment the grey matter of the medial temporal lobe and hippocampal subfields, and then computationally flatten out this tissue (see Ekstrom *et al.*, 2009; Zeineh *et al.*, 2003; and also in 7T MRI Suthana *et al.*, 2015). However, this protocol does not appear to capture subtle structural details and variations of the hippocampal head, such as its curvature and digitations. Furthermore, subfield segmentation was performed based on landmarks and geometric rules in the original space rather than based on the unfolded tissue, as implemented in the current protocol, with unfolding primarily used for visualization purposes. Unfolding protocols of this type face many of the same challenges as other manual segmentation protocols, and do not provide any sort of intrinsic alignment across participants. Nevertheless, they converges with the current work in demonstrating that tissue continuities and borders of the hippocampus and surrounding cortex can be visualized in a flattened plane in their full extent.

A final point worth noting is that the unfolded coordinate system offered here would also allow for easy implementation of further subfield divisions in future work. For example, Ding & Van Hoesen's recent characterization of the hippocampal head (2015), as well as other histological evidence from humans and non-human animals (see Ding, 2013), reveal differentiation of the subiculum into distinct components, specifically prosubiculum (postsubiculum in rodents), subiculum, presubiculum, and parasubiculum. Furthermore, some studies have documented functional differentiation between proximal and distal CA1 (Nakazawa *et al.*, 2016; Knierim *et al.*, 2014) and CA3 (Nakamura *et al.*, 2013). These findings highlight the increasing need for precision and standardization in indexing hippocampal tissue, as well as the need for flexibility in applying subfield labels so as to honour continuous new developments in tissue characterization. We believe that the unfolded coordinate system presented here can provide such a framework.

4 Conclusions

We have presented a new tool that promises to allow for *in vivo* characterization of the complex structure of the human hippocampal subfields in unprecedented detail. Manual segmentation with high anatomical detail poses many challenges for the generation of reliable protocols that are suitable for tracing of hippocampal subfields, in particular in the hippocampal head. However, considerations of regularities in hippocampal

structure related to ontogeny offer ways in which computational tools, such as the Laplace equation, can be applied for indexing and segmenting hippocampal tissue. In the current study we pursued an approach that took advantage of these considerations. Through computational unfolding of the hippocampus, the current protocol provides a coordinate system that can index hippocampal tissue in a precise and flexible manner, while capturing the noticeable inter-individual differences in morphology that have been documented in histological studies of this structure. This method critically depends on the visualization of the 'dark band' in order to distinguish folds of hippocampal archicortex. We argue that this method offers several practical advantages over manual segmentation techniques. These advantages can be summarized as follows:

i) Unfolding hippocampal grey matter allows for indexing of analogous tissues (or sets of candidate boundary locations) across participants with variable morphologies.

ii) Segmentations applied in this unfolded coordinate space show good spatial overlap with, and may even correct for tracing errors in, the detailed manual segmentations that were performed here for comparison. This coordinate system also captures subtle but critical structural features, as demonstrated in a direct comparison with a resected histological sample.

iii) The unfolded coordinate space described can be used for inter-subject alignment and subsequent mapping of properties across the full longitudinal and proximal-distal extents of the hippocampus, as illustrated here for intracortical myelin and cortical thickness measures.

Future directions for this work include the integration of automatic tissue segmentation tools for detection of dark band, grey matter, and surrounding structure in order to reduce user input and improve reliability. Promising applications of this unfolded coordinate system include cross-species comparison and normative mapping of hippocampal tissue properties in health and disease.

Acknowledgements

This project was supported by a CIHR Project Grant (Funding reference number: 148839), EpLink - The Epilepsy Research Program of the Ontario Brain Institute, and scanning was performed at Western's Centre for Functional and Metabolic Mapping, supported by the Canada First Research Excellence Fund to BrainsCAN.

References

Ábrahám, H., Vincze, A., Veszprémi, B., Kravják, A., Gömöri, É., Kovács, G. G., & Seress, L. (2012). Impaired myelination of the human hippocampal formation in Down syndrome. International Journal of Developmental Neuroscience, 30(2), 147-158.

Berron, D., P. Vieweg, A. Hochkeppler, J. B. Pluta, S-L. Ding, A. Maass, A. Luther et al. "A protocol for manual segmentation of medial temporal lobe subregions in 7tesla MRI." NeuroImage: Clinical (2017).

Blümcke, I., Pauli, E., Clusmann, H., Schramm, J., Becker, A., Elger, C., Merschhemke, M., Meencke, H.-J., Lehmann, T., von Deimling, A., Scheiwe, C., Zentner, J., Volk, B., Romstöck, J., Stefan, H., Hildebrandt, M., 2007. A new clinico-pathological classification system for mesial temporal sclerosis. Acta Neuropathol. 113, 235–244.

Dalton, M. A., Zeidman, P., Barry, D. N., Williams, E., & Maguire, E. A. (2017). Segmenting subregions of the human hippocampus on structural magnetic resonance image scans: An illustrated tutorial. Brain and Neuroscience Advances, 1, 2398212817701448.

Dice, L.R., 1945. Measures of the Amount of Ecologic Association Between Species. Ecology 26, 297–302.

Ding, S. L. (2013). Comparative anatomy of the prosubiculum, subiculum, presubiculum, postsubiculum, and parasubiculum in human, monkey, and rodent. Journal of Comparative Neurology, 521(18), 4145-4162.

Ding, S.-L., Van Hoesen, G.W., 2015. Organization and Detailed Parcellation of Human Hippocampal Head and Body Regions Based on a Combined Analysis of Cyto- and Chemoarchitecture. J. Comp. Neurol. 523, 2233–2253.

Duvernoy, H.M., Cattin, F., Risold, P.-Y., 2013. The Human Hippocampus: Functional Anatomy, Vascularization and Serial Sections with MRI, 4th edition.

Ekstrom, A.D., Bazih, A.J., Suthana, N.A., Al-Hakim, R., Ogura, K., Zeineh, M., Burggren, A.C., Bookheimer, S.Y., 2009. Advances in high-resolution imaging and computational unfolding of the human hippocampus. Neuroimage 47, 42–49.

Glasser, M.F., Goyal, M.S., Preuss, T.M., Raichle, M.E., Van Essen, D.C., 2014. Trends and properties of human cerebral cortex: correlations with cortical myelin content. Neuroimage 93 Pt 2, 165–175.

Glasser, M.F., Van Essen, D.C., 2011. Mapping human cortical areas in vivo based on myelin content as revealed by T1- and T2-weighted MRI. J. Neurosci. 31, 11597–11616.

Goubran, M., Crukley, C., de Ribaupierre, S., Peters, T.M., Khan, A.R., 2013. Image registration of *ex-vivo* MRI to sparsely sectioned histology of hippocampal and neocortical temporal lobe specimens. Neuroimage 83, 770–781. doi: 10.1002/ana.24318

Goubran, M., de Ribaupierre, S., Hammond, R.R., Currie, C., Burneo, J.G., Parrent, A.G., Peters, T.M., Khan, A.R., 2015. Registration of *in-vivo* to *ex-vivo* MRI of surgically resected specimens: a pipeline for histology to *in-vivo* registration. J. Neurosci. Methods 241, 53–65. doi: 10.1002/hbm.23090

Ho, N.F., Iglesias, J.E., Sum, M.Y., Kuswanto, C.N., Sitoh, Y.Y., De Souza, J., Hong, Z., Fischl, B., Roffman, J.L., Zhou, J., Sim, K., Holt, D.J., 2016. Progression from selective to general involvement of hippocampal subfields in schizophrenia. Mol. Psychiatry. doi:10.1038/mp.2016.4

Jenkinson, M., 2002. Improved Optimization for the Robust and Accurate Linear Registration and Motion Correction of Brain Images. Neuroimage 17, 825–841.

Jones, S.E., Buchbinder, B.R., Aharon, I., 2000. Three-dimensional mapping of cortical thickness using Laplace's Equation. Hum. Brain Mapp. 11, 12–32.

Kerchner, G.A., Hess, C.P., Hammond-Rosenbluth, K.E., Xu, D., Rabinovici, G.D., Kelley, D.A.C., Vigneron, D.B., Nelson, S.J., Miller, B.L., 2010. Hippocampal CA1 apical neuropil atrophy in mild Alzheimer disease visualized with 7-T MRI. Neurology 75, 1381–1387.

Knierim, J. J., Neunuebel, J. P., & Deshmukh, S. S. (2014). Functional correlates of the lateral and medial entorhinal cortex: objects, path integration and local–global reference frames. Phil. Trans. R. Soc. B, 369(1635), 20130369.

Marques, J. P., & Gruetter, R. (2013). New Developments and Applications of the MP2RAGE Sequence-Focusing the Contrast and High Spatial Resolution R 1 Mapping. PloS one, 8(7), e69294.

Nakamura, N. H., Flasbeck, V., Maingret, N., Kitsukawa, T., & Sauvage, M. M. (2013). Proximodistal segregation of nonspatial information in CA3: preferential recruitment of a proximal CA3-distal CA1 network in nonspatial recognition memory. Journal of Neuroscience, 33(28), 11506-11514.

Nakazawa, Y., Pevzner, A., Tanaka, K. Z., & Wiltgen, B. J. (2016). Memory retrieval along the proximodistal axis of CA1. Hippocampus, 26(9), 1140-1148.

Poppenk, J., Evensmoen, H.R., Moscovitch, M., Nadel, L., 2013. Long-axis specialization of the human hippocampus. Trends Cogn. Sci. 17, 230–240.

Sethian, J.A., 1999. Level Set Methods and Fast Marching Methods: Evolving Interfaces in Computational Geometry, Fluid Mechanics, Computer Vision, and Materials Science. Cambridge University Press.

Smith, E. (1897). The morphology of the indusium and straie lancisii. Anat Anz 13:23-27.

Sowell, E.R., Thompson, P.M., Leonard, C.M., Welcome, S.E., Kan, E., Toga, A.W., 2004. Longitudinal mapping of cortical

thickness and brain growth in normal children. J. Neurosci. 24, 8223–8231.

Suthana, N.A., Donix, M., Wozny, D.R., Bazih, A., Jones, M., Heidemann, R.M., Trampel, R., Ekstrom, A.D., Scharf, M., Knowlton, B., Turner, R., Bookheimer, S.Y., 2015. High-resolution 7T fMRI of Human Hippocampal Subfields during Associative Learning. J. Cogn. Neurosci. 27, 1194–1206.

Thomas, B.P., Welch, E.B., Niederhauser, B.D., Whetsell, W.O., Jr, Anderson, A.W., Gore, J.C., Avison, M.J., Creasy, J.L., 2008. High-resolution 7T MRI of the human hippocampus in vivo. J. Magn. Reson. Imaging 28, 1266–1272.

Tofts, P., 2005. Quantitative MRI of the Brain: Measuring Changes Caused by Disease. John Wiley & Sons.

Williams, P.L., 1995. Gray's Anatomy: The Anatomical Basis of Medicine and Surgery.

Winterburn, J.L., Pruessner, J.C., Chavez, S., Schira, M.M., Lobaugh, N.J., Voineskos, A.N., Mallar Chakravarty, M., 2013. A novel in vivo atlas of human hippocampal subfields using high-resolution 3T magnetic resonance imaging. Neuroimage 74, 254–265.

Wisse, L.E.M., Daugherty, A.M., Olsen, R.K., Berron, D., Carr, V.A., Stark, C.E.L., Amaral, R.S.C., Amunts, K., Augustinack, J.C., Bender, A.R., Bernstein, J.D., Boccardi, M., Bocchetta, M., Burggren, A., Chakravarty, M.M., Chupin, M., Ekstrom, A., de Flores, R., Insausti, R., Kanel, P., Kedo, O., Kennedy, K.M., Kerchner, G.A., LaRocque, K.F., Liu, X., Maass, A., Malykhin, N., Mueller, S.G., Ofen, N., Palombo, D.J., Parekh, M.B., Pluta, J.B., Pruessner, J.C., Raz, N., Rodrigue, K.M., Schoemaker, D., Shafer, A.T., Steve, T.A., Suthana, N., Wang, L., Winterburn, J.L., Yassa, M.A., Yushkevich, P.A., la Joie, R., Hippocampal Subfields Group, 2017. A harmonized segmentation protocol for hippocampal and parahippocampal subregions: Why do we need one and what are the key goals? Hippocampus. doi: 10.1002/hipo.22671

Wisse, L., Gerritsen, L., Kuijf, H., Zwanenburg, J., Koek, H., Luijten, P., Biessels, G.-J., Geerlings, M., 2011. Hippocampal subfields at 7T MRI: In vivo volumetric assessment. Alzheimers. Dement. 7, e42.

Yushkevich, P.A., Amaral, R.S.C., Augustinack, J.C., Bender, A.R., Bernstein, J.D., Boccardi, M., Bocchetta, M., Burggren, A.C., Carr, V.A., Chakravarty, M.M., Chételat, G., Daugherty, A.M., Davachi, L., Ding, S.-L., Ekstrom, A., Geerlings, M.I., Hassan, A., Huang, Y., Iglesias, J.E., La Joie, R., Kerchner, G.A., LaRocque, K.F., Libby, L.A., Malykhin, N., Mueller, S.G., Olsen, R.K., Palombo, D.J., Parekh, M.B., Pluta, J.B., Preston, A.R., Pruessner, J.C., Ranganath, C., Raz, N., Schlichting, M.L., Schoemaker, D., Singh, S., Stark, C.E.L., Suthana, N., Tompary, A., Turowski, M.M., Van Leemput, K., Wagner, A.D., Wang, L., Winterburn, J.L., Wisse, L.E.M., Yassa, M.A., Zeineh, M.M., Hippocampal Subfields Group (HSG), 2015a. Quantitative comparison of 21 protocols for labeling hippocampal subfields and parahippocampal subregions in in vivo MRI: towards a harmonized segmentation protocol. Neuroimage 111, 526–541.

Yushkevich, P.A., Avants, B.B., Pluta, J., Das, S., Minkoff, D., Mechanic-Hamilton, D., Glynn, S., Pickup, S., Liu, W., Gee, J.C., Grossman, M., Detre, J.A., 2009. A high-resolution computational atlas of the human hippocampus from postmortem magnetic resonance imaging at 9.4 T. Neuroimage 44, 385–398.

Yushkevich, P.A., Piven, J., Hazlett, H.C., Smith, R.G., Ho, S., Gee, J.C., Gerig, G., 2006. User-guided 3D active contour segmentation of anatomical structures: significantly improved efficiency and reliability. Neuroimage 31, 1116–1128.

Yushkevich, P.A., Pluta, J.B., Wang, H., Xie, L., Ding, S.-L., Gertje, E.C., Mancuso, L., Kliot, D., Das, S.R., Wolk, D.A., 2015b. Automated volumetry and regional thickness analysis of hippocampal subfields and medial temporal cortical structures in mild cognitive impairment. Hum. Brain Mapp. 36, 258–287.

Yushkevich P. A., H. Wang, J. Pluta , S. R. Das , B. Avants , M. Weiner , S. Mueller , and D. Wolk. (2011). Measuring the volumes and thickness of hippocampal subfields in vivo using automatic segmentation of T2-weighted MRI: A pilot evaluation study Proc. Intl. Soc. Mag. Reson. Med. 19

Zeidman, P., Maguire, E.A., 2016. Anterior hippocampus: the anatomy of perception, imagination and episodic memory. Nat. Rev. Neurosci. 17, 173–182.

Zeineh, M.M., Engel, S.A., Thompson, P.M., Bookheimer, S.Y., 2003. Dynamics of the hippocampus during encoding and retrieval of face-name pairs. Science 299, 577–580.